ISSN 1070-3284, Russian Journal of Coordination Chemistry, 2013, Vol. 39, No. 5, pp. 405–410. © Pleiades Publishing, Ltd., 2013.

A Ytterbium Polymer Incorporating Ethyl-4,5-Imidazole-Dicarboxylate and Formate Coligand: Structure, Luminescent, and Magnetic Properties[1]

X. Feng[a], Y. Zhao[c], P. P. Lei[a], J. J. Shang[a], and L. Y. Wang[a, b, *]

[a] *College of Chemistry and Chemical Engineering, Luoyang Normal University, Luoyang, 471022 P.R. China*

[b] *College of Chemistry and Pharmacy Engineering, Nanyang Normal University, Nanyang, 473601 P.R. China*

[c] *College of Physics and Electronic Information, Luoyang Normal University, Luoyang, 471022 P.R. China*

**e-mail: wlya@lynu.edu.cn*

Received September 24, 2011

Abstract—A new lanthanide-organic coordination polymer incorporating both substituted imdazole dicarboxylate and formate auxiliary ligand, namely $\{[Yb_3(HEimda)_4(\mu_2\text{-}HCOO) \cdot 4H_2O] \cdot 2H_2O\}_n$ (**I**) (H_3Eimda = 1*H*-2-ethyl-4,5-imidazole-dicarboxylic acid), has been prepared and was structurally characterized by elemental analysis, IR and X-ray diffraction. It crystallizes in the monoclinic system, space group of *C*2/*c*. The polymer **I** is built from two dimensional (2D) double decker networks based on the $Ln_4HEimda_4$ tetranuclear basic carboxylate as secondary building unit. The extensive hydrogen bonds extend the 2D lamellar network into a 3D supramolecular aggregate. The emission spectrum of polymer **I** exhibits ligand-to-metal charge-transfer luminescence. Variable-temperature magnetic susceptibility measurement reveals that the end to end bridging fashion of formate group results in the depopulation of the stark levels for a single Yb^{3+} ion and/or possible antiferromagntic interactions between Yb^{3+} ions within the carboxylato bridged dinuclear unit.

DOI: 10.1134/S1070328413050023

INTRODUCTION

In recent years, the design and construction of extended frameworks containing rare-earth metals bridged by carboxylic groups have attracted a great deal of interest in chemistry and materials science fields, owing to their extraordinary molecular architectures and fascinating chemical/physical properties [1–4]. Over the last decades, a variety of multicarboxylate triazine/imidazoline/pyridine-based ligands have been extensively employed for exhibiting various coordination fashions to accompany diversity of interesting structures with honeycomb, rectangular grid, bilayer lattice, 1D ladder and diamonds frameworks, with gas adsorptions, magnetic and luminescent properties, and so on [5]. However, among various strategies, most of the work has focused on the assembly of the *d*-block metal-organic frameworks, and the analogous chemistry of the lanthanide ions still remains less developed [6]. It has also been demonstrated that formate, being the smallest carboxylate, is cheap and with low toxicity, and it has a small stereo effect which is beneficial for constructing of metal-organic frameworks (MOFs) [7]. Meanwhile, formate ligand plays an important role in coordination chemistry, which may adopt a remarkable versatile three-atom binding modes such as monodentate, chelating, and bridging in the *syn–syn, syn–anti,* and *anti–anti* configurations [8, 9]. As a continuation of our previous investigation and better understand the influence exerted by the formate auxiliary ligand on the structures and properties in these systems, we describe here the synthesis, structure, photoluminescence, and magnetic properties of a ytterbium-organic polymer $\{[Yb_3(HEimda)_4(\mu_2\text{-}HCOO) \cdot 4H_2O] \cdot 2H_2O\}_n$ (**I**) based on the 1*H*-2-ethyl-4,5-imidazole-dicarboxylate (HEimda) and formate ligand. It is also hoped that the combination of two types of ligands will enhance the energy-transfer efficiency from ligand to lanthanide ions [10].

EXPERIMENTAL

Materials and physical measurements. All reagents used in the syntheses were of analytical grade and used as received. Elemental analyses for C, H, and N were performed on a Vario EL III elemental analyzer. The infrared spectra (4000–400 cm^{-1}) were recorded by using KBr pellet on an AvatarTM 360 E.S.P. IR spectrometer. Thermogravimetry-differential thermal analysis was recorded using a SDT 2960 simultaneous thermal analyzer (DTA Instruments, New Castle, DE) in N_2 atmosphere at a heating rate of 10°C min^{-1} from 20 to 900°C. Luminescence spectra of polymer **I** in a 1 cm quartz spectrophotometer fluorescence cell (Starna) in methanol were run on a Cary Eclipse fluores-

[1] The article is published in the original.

Table 1. Crystal data and structure refinement details for the polymer **I**

Parameter	Value
Formula weight	1400.79
Temperature	296(2)
Crystal system	Monoclinic
Space group	$C2/c$
a, Å	33.620(3)
b, Å	9.1156(9)
c, Å	12.9595(13)
β, deg	92.0560(10)
V, Å^3	3969.1(7)
Z	4
ρ, g cm^{-3}	2.344
Crystal size, mm	0.23 × 0.18 × 0.15
F(000)	2676
μ, mm^{-1}	7.114
θ Range for data collection, deg	2.32–25.50
Limiting indice rangs	$-40 \le h \le 40$, $-11 \le k \le 11$, $-15 \le l \le 15$
Type of scan	φ/ω
Reflections collected	14234
Independent reflections (R_{int})	3684
Reflections with $I > 2\sigma(I)$	3627
Max and min transmissions	0.4150 and 0.2915
Name of parameters	297
GOOF	1.041
R_1, wR_2 ($I > 2\sigma(I)$)	0.0359, 0.1224
R_1, wR_2 (all data)	0.0363, 0.1229
$\Delta\rho_{max}$ and $\Delta\rho_{min}$, e Å^{-3}	1.734 and −2.701

Note: $R = [\Sigma||F_o| - |F_c||/\Sigma|F_o|]$, $R_W = \Sigma_W[|F_o^2 - F_c^2|^2/\Sigma_W(|F_w|^2)^2]^{1/2}$.

cence spectrophotometer. Variable-temperature magnetic susceptibilities were measured using a MPMS-7 SQUID magnetometer under a 0.2 T applied magnetic field and over the range of 2 to 300 K. Diamagnetic corrections were made with Pascal's constants for all constituent atoms.

Synthesis of the polymer I. H_3Eimda acid (0.039 g, 0.2 mmol) and sodium formate dihydrate (0.021 g, 0.2 mmol) in a solution of water–alcohol (v/v = 1.2, 10 mL) were mixed with an aqueous solution (10 mL) of $Yb(NO_3)_3 \cdot 6H_2O$ (0.089 g, 0.2 mmol). After stirring for 20 min in air, the pH value was adjusted to 3.5 with nitric acid, and the mixture was placed into 25 mL Teflon-lined autoclave under autogenous pressure being heated at 155°C for 72 h, then the autoclave was cooled over a period of 24 h at a rate 5°C/h. After filtration, the product was washed with distilled water and then dried, colorless crystals of **I** were obtained suitable for X-ray diffraction analysis. The yield was 0.0362 g (39%) based on lanthanide element.

For $C_{29}H_{37}N_8O_{24}Yb_3$

anal. calcd., %:	C, 26.14;	H, 2.79;	N, 8.41.
Found, %:	C, 26.25;	H, 2.76;	N, 8.28.

IR (KBr; ν, cm^{-1}): 3384 s, 3186 br, 2978 m, 1590 s, 1529 s, 1462 s, 1410 m, 1338 s, 1279 m, 1212 s, 867 m, 810 v.s, 793 s, 660 s, 569 m.

Crystallographic data collection and refinement. Single-crystal diffraction data of complex **I** were collected on a Bruker SMART APEX CCD diffractometer with graphite-monochromated MoK_α radiation (λ = 0.71073 Å) at room temperature. The structure was solved using direct methods and successive Fourier difference synthesis (SHELXS-97) [11] and refined using the full-matrix least-squares method on F^2 with anisotropic thermal parameters for all nonhydrogen atoms (SHELXL-97) [12]. The disordered ethyl carbon atoms of HEimda ligand and formate oxygen atoms were restrained in order to obtain reasonable thermal parameters. The hydrogen atoms of organic ligands were placed in calculated positions and refined using a riding on attached atoms with isotropic thermal parameters 1.2 times those of their carrier atoms. The summary crystallographic data and selected bond lengths and angles for polymer **I** are listed in Table 1 and 2, respectively.

Supplementary material for structure **I** has been deposited with the Cambridge Crystallographic Data Centre (no. 845838; deposit@ccdc.cam.ac.uk or http://www.ccdc.cam.ac.uk).

RESULTS AND DISCUSSION

Polymer **I** is a lanthanide-organic 3D framework based on lanthanide-organic square motifs. As illustrated in Fig. 1a, the asymmetric unit of **I** contains three crystallographically independent Yb^{3+} cations, three HEimda ligands, one formate group, and four coordinated waters, as well as two lattice water molecules. All of three HEimda anion ligands have the same coordination mode with dangling lateral ethyl arms, chelating three Yb^{3+} ions. Interestingly, the asymmetric coordination pattern of the ligand led to a crystal structure belonging to a centric space group. There are two categories of Yb^{3+} ions in the unit and both categories of the Yb^{3+} ions are in an octacoordinate manner, exhibiting a slightly distorted square antiprism geometry, but with different coordination environments. The Yb(1) ion is coordinated with two imidazolyl nitrogen atoms from the HEimda ligands, five carboxylate oxygen atoms from the HEimda ligands, and the coordination sphere of the Yb(1) cat-

Table 2. Selected bond lengths (Å) and bond angles (deg) for polymer **I***

Bond	*d*, Å	Bond	*d*, Å	Bond	*d*, Å
Yb(1)–O(6)$^{\#2}$	2.232(6)	Yb(1)–O(1)	2.344(5)	Yb(2)–O(2)$^{\#4}$	2.243(6)
Yb(1)–O(7)$^{\#2}$	2.280(6)	Yb(1)–O(9)	2.354(7)	Yb(2)–O(12)$^{\#4}$	2.332(16)
Yb(1)–O(8)	2.304(5)	Yb(1)–N(1)	2.506(6)	Yb(2)–O(10)$^{\#4}$	2.336(7)
Yb(1)–O(4)$^{\#3}$	2.310(6)	Yb(2)–O(10)	2.336(7)	Yb(2)–O(3)	2.363(6)
Angle	ω, deg	Angle	ω, deg	Angle	ω, deg
O(6)$^{\#2}$Yb(1)O(7)$^{\#2}$	77.2(2)	O(7)$^{\#2}$Yb(1)O(9)	73.6(3)	O(4)$^{\#3}$Yb(1)N(3)	121.8(2)
O(6)$^{\#2}$Yb(1)O(8)	106.4(2)	O(8)Yb(1)O(9)	89.5(3)	O(1)Yb(1)N(3)	75.8(2)
O(6)$^{\#2}$Yb(1)O(4)$^{\#3}$	79.1(3)	O(4)$^{\#3}$Yb(1)O(9)	74.0(2)	O(9)Yb(1)N(3)	143.4(2)
O(7)$^{\#2}$Yb(1)O(4)$^{\#3}$	76.8(2)	O(1)Yb(1)O(9)	70.6(2)	N(1)Yb(1)N(3)	81.5(2)
O(8)Yb(1)O(4)$^{\#3}$	75.0(2)	O(6)$^{\#2}$Yb(1)N(1)	94.0(3)	O(2)$^{\#4}$Yb(2)O(2)	89.8(4)
O(6)$^{\#2}$Yb(1)O(1)	144.6(2)	O(7)$^{\#2}$Yb(1)N(1)	74.1(2)	O(2)Yb(2)O(3)$^{\#4}$	144.9(2)
O(7)$^{\#2}$Yb(1)O(1)	121.4(2)	O(8)Yb(1)N(1)	133.6(2)	O(2)Yb(2)O(12')$^{\#5}$	84.1(5)
O(8)Yb(1)O(1)	72.9(2)	O(1)Yb(1)N(1)	66.8(2)	O(12)Yb(2)O(3)	128.9(4)
O(7)$^{\#2}$Yb(1)N(3)	138.9(2)	O(6)$^{\#2}$Yb(1)N(3)	72.0(2)	O(2)Yb(2)O(12')$^{\#1}$	76.6(5)
O(2)$^{\#4}$Yb(2)O(12)	72.8(6)	O(8)Yb(1)N(3)	66.8(2)	O(2)Yb(2)O(12)$^{\#4}$	72.8(6)
O(2)Yb(2)O(12)	67.6(5)	O(7)$^{\#2}$Yb(1)O(8)	150.2(2)	O(12)$^{\#4}$Yb(2)O(3)	77.4(5)

* Symmetry codes: $^{\#1}$ $-x+1, -y+1, -z+1$; $^{\#2}$ $x, -y, z-1/2$; $^{\#3}$ $x, y-1, z$; $^{\#4}$ $-x+1, y, -z+1/2$; $^{\#5}$ $x, -y+1, z-1/2$; $^{\#6}$ $x, y+1, z$; $^{\#7}$ $x, -y, z+1/2$.

ion is completed by one oxygen atom from terminal water molecule with a $Yb_1O_6N_2$ sphere, whereas the Yb(2) ion is surrounded by four oxygen atoms from carboxylate groups of HEimda ligands and two oxygen atoms from bridging formate groups, two oxygens of the water molecules.

The dihedral angles between the neighboring HEimda ligands sharing the one Yb^{3+} ion are 86.25° and 14.80°, respectively, and the H_3Eimda is deprotonated completely acting as a pentadentate ligand. It displays μ_3-*k*N, O: *k*O, O': *k*O' fashion to connect three Yb^{3+} ions.

The dinuclear units linked by HEimda and formate in polymer **I** are illustrated as follows:

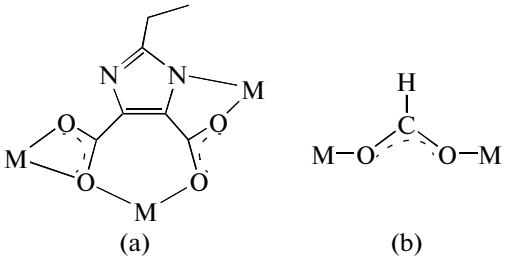

(a) (b)

Scheme.

Both two carboxyl groups adopt the bis-(bridging) bidentate and monodentate modes (Scheme, a). Each HEimda ligand employs the 4-carboxylate group oxygen (O(2)) and 5-carboxylate group oxygen (O(3)) to chelate the Yb(2) ion. The two neighboring Yb(1) ions are linked via 5-carboxylate group oxygen and 3-imidazole nitrogen of the HEimda simultaneously to produce a Yb_2 diunclear unit with the Yb···Yb separation of 6.61(8) Å. These dinuclear segments are grafted on

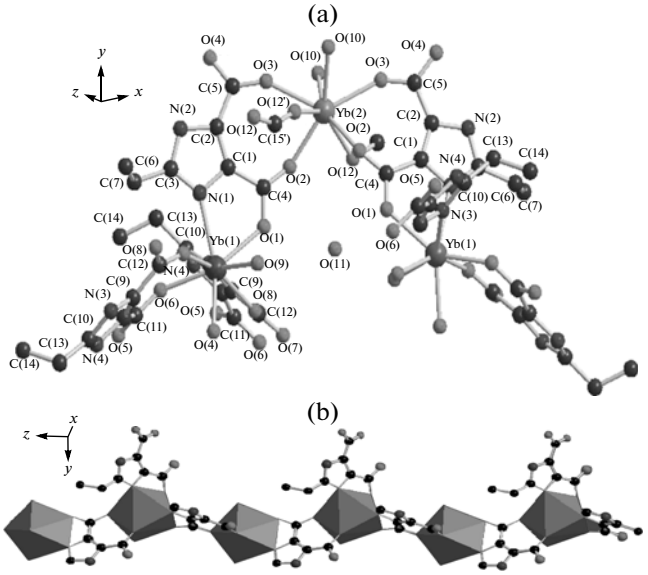

Fig. 1. The coordination environments of Yb^{3+} ions in **I** along *xy* plane. Hydrogen atoms and free water molecules have been omitted for clarity (a); polyhedral diagram of the 1D alternate chain of Yb(1) cations linked by the HEimda ligand viewed along *z* axis in **I** (b).

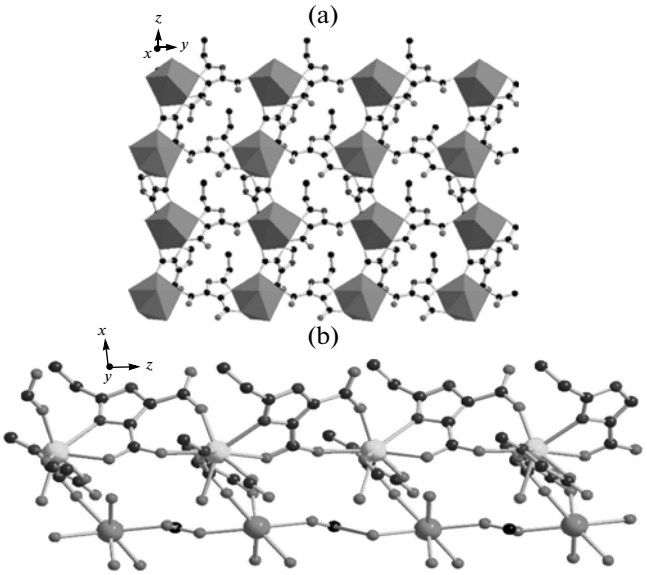

Fig. 2. Diamond illustration of the monolayer 2D (4,4) corrugated layers in **I** along the *z* axis (H atoms and free waters are not included for clarity) (a); the linear double chain network of Heimda-linking up Yb(III) atoms as viewed along the *y* axis (b).

to a 1D infinite ribbon chain array along the crystallographic *z* axis (Fig. 1b). Moreover, the third HEimda ligand acts as a linker using the 4-carboxylate oxygen and its symmetric partners consequently propagate these 1D chains into an interesting corrugated lamellar framework along the *xy* plane, as displayed in Fig. 2a, in which the adjacent binuclear units are connected together by the μ_2-O bridge from 5-carboxylate group of the HEimda ligand to generate a parallelogram arrangement composed of four Yb(1) ions, and the diagonal-to-diagonal distances are 6.51, 6.62 Å, respectively. The individual nets are undulated and sinusoidal in nature, and due to parallel of two nets the standing wavelike 4,4 order topology layers arises [13]. Meantime, bridging formate groups in polymer **I** interlink neighboring Yb(2) ions in an end to end (*anti–anti*) fashion, resulting in an infinite 1D $\{[Yb(HCOO)]^{2+}\}_n$ chain (Scheme, b) oriented parallel to the *z* crystal direction, which is similar to many related compounds with formate as a bridging ligand, thus it is interesting to perform magnetic studies that evaluate the eventual exchange interactions between the metal centers. The Yb(2)···Yb(2) separation is 6.862 Å within the chain, and the $\{[Yb(HCOO)]^{2+}\}_n$ chains parallel to the $\{[Yb(HEimda)]^{+}\}_n$ chain above mentioned constructed by the HEimda ligand, giving rise to the 1D double chain along *xz* plane, as displayed in Fig. 2b. The adjacent 2D coordination networks are further interlinked by the Yb(2) formate chains tectonics via the 5-carboxylate groups from the third Heimda to fabricate a claylike double layer [14] complicated coordination frameworks consequently, as demonstrated in Fig. 3.

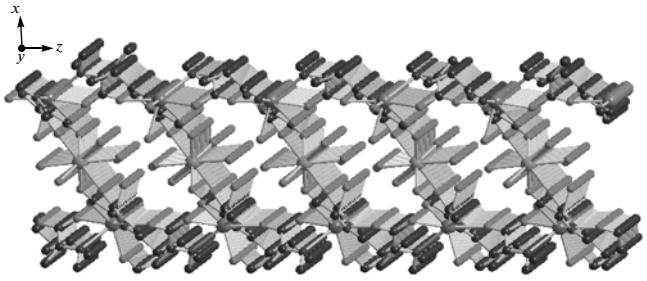

Fig. 3. Projective view of 2D double-decker motif consisting of two mono-layers connected by HEimda ligands along *xz* plane.

These double layers are further stacked together and extended into 3D supramolecular edifice through the strong interlayer hydrogen interactions between dicarboxylate group and imidazole rings from the adjacent 2D double sheets N(4)–H(4)...O(5)$^{\#8}$ (O–N 2.755(1) Å, O···H–N 166°). The extensive hydrogen bonding interactions play very important role for the formation and stabilization of these supramolecular frameworks, and the distance between the adjacent layers is about 8.60 Å. This array may be comparable to the series of lanthanide coordination polymers containing the 5-pyrazoledicarboxyl ate with the same crystal system [15].

However, the coordination fashions of the formate in this work differs essentially from those of analogous transition metal complexes, in which the formate also acts as a linker to further extend the dimension to a 3D networks by covalent bonds [16].

The TG diagram of **I** exhibits an initial mass loss of 7.81% corresponding to start with the departure of the coordinated and uncoordinated water molecules, and the decomposition of **I** begins above 260°C (Fig. 4), which is attributed to the release of the formate groups (calcd. 3.40%). The compound begin to decompose

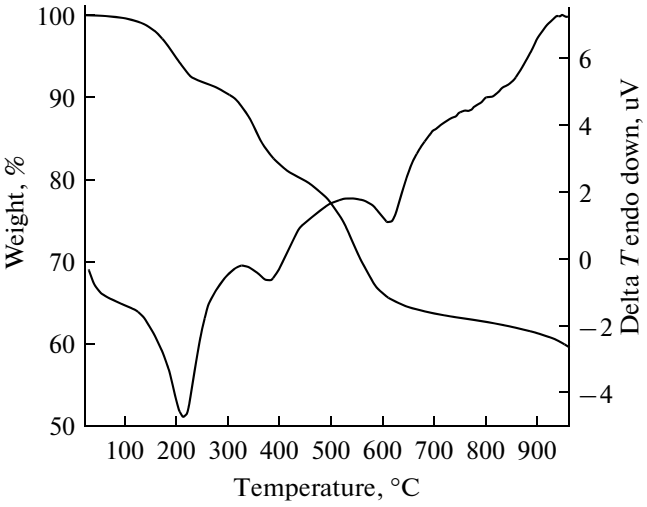

Fig. 4. The TG–DTA curves for polymer **I**.

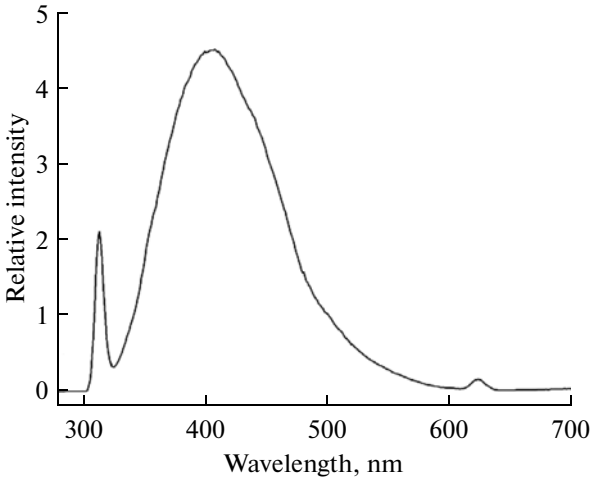

Fig. 5. The liquid photo emission spectra of $\{[Yb_3(HEimda)_4(\mu_2\text{-}HCOO) \cdot 4H_2O] \cdot 2H_2O\}_n$ under the UV excitation with the samples dispersed in the methanolic suspension at room temperature.

upon further heating and underwent a rapid and significant weight loss of ~33% in the temperature range of 450–550°C, which corresponds to the destruction of the HEimda ligands (calcd. 34%).

The photoluminescence property of the methanolic suspension sample (~0.005 mol/L) of **I** was investigated at room temperature upon photoexcitation with 313 nm, as reported in Fig. 5. The emission spectra of polymer **I** not only consists narrow and sharp emission with the maximum wavelength of $\lambda_{max} = 315$ nm, but also the sharp line spectrum of 415 nm. The former emission can be assigned to the π–π^* or n–n^* intraligand fluorescence. The later highest intense fluorescent emission band with $\lambda_{max} = 415$ nm would be attributed to the formation of ligand-to metal charge transfer (LMCT) transition, based on the emission spectrum of the free ligand [17].

Variable-temperature magnetic susceptibility measurements were performed on microcrystalline samples given polymer **I**. The temperature dependence of the magnetic susceptibility of polymer **I** is reported in Fig. 6. The $\chi_M T$ value of **I** is 5.46 cm^3 K mol^{-1} at 300 K, which is somewhat larger than the expected spin-only value for two independent spins $S = 1/2$ (with $^2F_{7/2}$ ground multiplet state, 4.54 μ_B, $g = 8/7$) [18] and is very close to the value of Yb(III) complex with L-alanine ligand [19]. When the temperature was cooled to 2.0 K, the $\chi_M T$ decreases gradually monotonically to a value of 2.58 cm^3 K mol^{-1}, which is similar to those of other reported Yb(III) Double-decker phthalocyanine complexes [18]. The $\chi_M T$ decreases with the temperature, what is also a result of Kramers degeneration of lanthanide levels and antiferromagnetic correlations. But very large orbital moments of the ytterbium ion additionally complicate the analysis of magnetic data [20].

ACKNOWLEDGMENTS

We are grateful to the National Natural Science Foundation of China (nos. 21071074 and 21273101), Program for Backbone Teachers in Universities of Henan university (no. 2012GGJS-158), and the Natural Science Foundation of Education Committee of

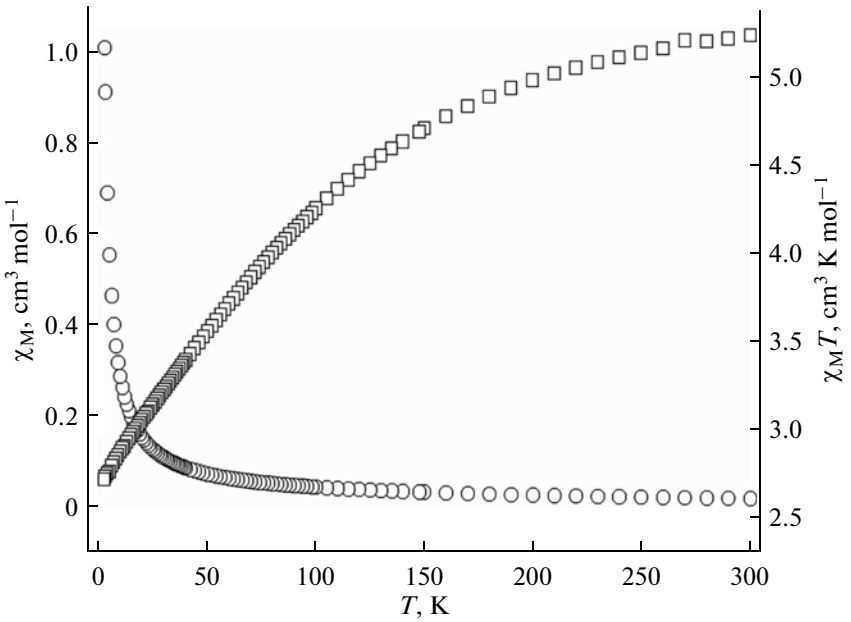

Fig. 6. Experimental magnetic data plotted as $\chi_M T$ (□) and χ_M (○) for $\{[Yb_3(HEimda)_4(\mu_2\text{-}HCOO) \cdot 4H_2O] \cdot 2H_2O\}_n$ under an applied field of 0.2 T between 2 and 300 K.

Henan, China (no. 2011B150022) for financial support of this work.

REFERENCES

1. Lee, W.R., Ryu, D.W., et al., *Inorg. Chem*., 2010, vol. 49, no. 11, p. 4723.
2. Feng, X., Zhao, J.S., Liu, B., et al., *Cryst. Growth Des*., 2010, vol. 10, no. 4, p. 1399.
3. Kumar, D.K., Das, A., and Dastidar, P., *Cryst. Growth Des*., 2007, vol. 7, no. 2, p. 205.
4. Shu, M.H., Tu, C.L., Xu, W.D., et al., *Cryst. Growth Des*., 2006, vol. 6, no. 8, p. 1890.
5. Nonat, A.M., Allain, C., Faulkner, S., and Gunnlaugsson, T., *Inorg. Chem*., 2010, vol. 49, no. 18, p. 8449.
6. Férey, G., Mellot-Draznieks, C., Serre, C., et al., *Science*, 2005, vol. 309, no. 5743, p. 2040.
7. Hong, M.C., Zhao, Y.J., Su, W.P., et al., *Angew. Chem. Int. Ed.*, 2000, vol. 39, no. 14, p. 2468.
8. Li, B., Gu, W., Zhang, L.Z., et al., *Inorg. Chem*., 2006, vol. 45, no. 26, p. 10425.
9. Luo, F., Long, G.J., Che, Y.X., and Zheng, J.M., *Cryst. Growth Des*., 2008, vol. 8, no. 10, p. 3511.
10. Kajiwara, T., Hasegawa, M., Ishii, A., et al., *Eur. J. Inorg. Chem*., 2008, vol. 36, p. 5565.
11. Sheldrick, G.M., *SHELXS-97, Program for the Solution of Crystal Structure*, Göttingen (Germany): Univ. of Göttingen, 1997.
12. Sheldrick, G.M., *SHELXL-97, Program for the Crystal Structure Refinement*, Göttingen (Germany): Univ. of Göttingen, 1997.
13. Feng, X., Zhang, G., Zhang, R.L., et al., *Chin. J. Struct. Chem*., 2011, vol. 30. no. 1, p. 144.
14. Wang, X.Y., Gan, L., Zhang, S.W., and Gao, S., *Inorg. Chem*., 2004, vol. 43, no. 15, p. 4615.
15. Xia, J., Zhao, B., Wang, H.S., et al., *Inorg. Chem*., 2007, vol. 46, no. 9, p. 3450.
16. Zhang, X.J., Xing, Y.H., Han, J., et al., *Cryst. Growth Des*., 2008, vol. 8, no. 10, p. 3680.
17. Feng, X., Liu, B., Wang, L.Y., et al., *Dalton Trans*., 2010, vol. 39, p. 8038.
18. Ishikawa, N., Iino, T., and Kaizu, Y., *J. Phys. Chem*., *A*, 2002, vol. 106, no. 41, p. 9543.
19. Puchalska, M., Mroziński, J., and Legendziewicz, J., *J. Alloys Compd*., 2008, vol. 451, no. 1, p. 270.
20. Hernández-Molina, M., Lorenzo-Luis, P.A., Lópeza, T., et al., *CrystEngComm*., 2000, vol. 2, no. 31, p. 169.